ARTICLE

OPEN

Check for updates

Spin-orbit torque switching of chiral magnetization across a synthetic antiferromagnet

Kang Wang [1✉], Lijuan Qian[1], See-Chen Ying[1] & Gang Xiao [1✉]

The interfacial Dzyaloshinskii-Moriya interaction (DMI) holds promises for design and control of chiral spin textures in low-dimensional magnets with efficient current-driven dynamics. Recently, an interlayer DMI has been found to exist across magnetic multilayers with a heavy-metal spacer between magnetic layers. This opens the possibility of chirality in these three-dimensional magnetic structures. Here we show the existence of the interlayer DMI in a synthetic antiferromagnetic multilayer with both inversion and in-plane asymmetry. We analyse the interlayer DMI's effects on the magnetization and the current-induced spin-orbit torque (SOT) switching of magnetization through a combination of experimental and numerical studies. The chiral nature of the interlayer DMI leads to an asymmetric SOT switching of magnetization under an in-plane magnetic field. Our work paves the way for further explorations on controlling chiral magnetizations across magnetic multilayers through SOTs, which can provide a new path in the design of SOT devices.

[1] Department of Physics, Brown University, Providence, RI 02912, USA. ✉email: kang_wang@brown.edu; gang_xiao@brown.edu

The Dzyaloshinskii–Moriya interaction (DMI) is an anti-symmetric interaction between two spins that originates from indirect exchange interaction mediated by intermediate nonmagnetic atoms with large spin–orbit coupling. The interfacial DMI discovered at the interface between a magnetic layer and a heavy-metal layer promotes chirality of magnetic domain walls[1,2], favoring one sense of rotation of the magnetization over the other. This allows the possibility of topological spin textures such as magnetic skyrmions to be found in low-dimensional magnets[3–7]. Recently, a theoretical work predicted that an interlayer DMI is also present between two magnetic layers in a synthetic antiferromagnet (SAF) separated by a heavy-metal spacer[8]. The interlayer DMI can give rise to a chiral magnetization across magnetic multilayers, which have been experimentally observed in some prototype systems[9–11]. The interlayer DMI, together with the interfacial DMI, can eventually lead to three-dimensional (3D) chiral spin textures, with possible applications in magnetic memory and spin logic devices.

Spin currents can exert spin torques on magnetization, enabling the manipulation of magnetization more efficiently than magnetic field-based controls. Most research efforts so far have focused on using spin currents to manipulate chiral magnetic domain walls and 2D topological spin textures in magnetic configurations arising from the interfacial DMI[4,12–17]. Fast motion of chiral magnetic domain walls and skyrmions has been reported in magnetic thin films[4,12,15–17]. The effective field of the interfacial DMI alternates in direction between successive magnetic domain walls. This induces a chiral spin torque, giving rise to a domain-wall motion with different velocities upon the influence of in-plane magnetic fields in opposite directions[15,17]. The chirality-induced nonreciprocity, defined here as different behaviors of a system in response to opposite excitations, is a universal phenomenon. For example, in a recently discovered superconducting diode, Cooper pairs can transport in a direction-selective manner under the interfacial Rashba effect[18]. One expects that the interlayer DMI-controlled chirality of magnetization would also induce certain nonreciprocal phenomena of great interest. It has been experimentally shown that the magnetic field-driven switching of the magnetization is asymmetric with the application of an additional orthogonal magnetic field[9,10], while the spin-current effect on the interlayer DMI-controlled chiral magnetization has not yet been studied.

In this paper, we report experimental and theoretical investigations of the spin torque-driven switching of the interlayer DMI-controlled chiral magnetization in a SAF structure. The interlayer exchange coupling (IEC) in the SAF has both a symmetric and an antisymmetric component that competes with magnetic anisotropy energies, determining the resultant magnetic configuration in the structure. The symmetric part of the IEC is the well-known Ruderman–Kittel–Kasuya–Yosida (RKKY) interaction[19–25]. Its sign is oscillatory depending on the spacer thickness. The antisymmetric part is responsible for the interlayer DMI that causes an asymmetric current-driven switching of the chiral magnetization across magnetic multilayers. The asymmetric current-driven switching is on account of the spin torque arising from the interlayer DMI with the chiral nature, which provides a new function in controlling magnetic textures in magnetic multilayers.

Results
Fabrication of the SAF with the interlayer DMI. For our study, we fabricated a SAF with the structure of $Ta(4.0)/MgO(1.6)/Co_{40}Fe_{40}B_{20}(1.1)/Ta(1.6)/Co_{40}Fe_{40}B_{20}(0.9)/MgO(1.6)/TaO_x(2.0)$ (layer thicknesses in nanometers) that breaks inversion symmetry normal to the layers. The multilayers were deposited on thermally oxidized silicon wafers using a high-vacuum magnetron

sputtering system (see "Methods" for details). After deposition, we used photolithography and physical ion milling to pattern the films into Hall bars with 140-μm-long and 20-μm-wide stripes. The samples were then annealed in a high-vacuum chamber at 210 °C for 1 h. During the annealing process, a perpendicular magnetic field of ~0.4 T was applied.

In the SAF structure, the bottom Ta(4.0) layer is a buffer layer. MgO layers promote perpendicular magnetic anisotropies of neighboring ferromagnetic $Co_{40}Fe_{40}B_{20}$ layers[26,27]. The top $Co_{40}Fe_{40}B_{20}$ layer has a stronger perpendicular magnetic anisotropy, while magnetization in the thicker bottom $Co_{40}Fe_{40}B_{20}$ layer is near the spin transition between perpendicular and in-plane reorientation[25]. The Ta layer as a spacer has a large spin Hall angle[28,29], which allows efficient conversion of a charge current to a spin current. In addition, the Ta spacer provides a weak symmetric IEC between magnetic layers[25,30]. The weak symmetric IEC, together with weak anisotropies of magnetic layers, facilitates the observation of the interlayer DMI's effects on magnetization and its switching by spin-current-induced spin–orbit torques (SOTs).

To obtain a finite interlayer DMI in our SAF, we introduced a spatial variation of IEC by fabricating both wedge-shaped Ta spacer and $Co_{40}Fe_{40}B_{20}$ layers. This was achieved by placing substrates with an off-centered displacement relative to the center of the circular sputter source. The deposition is in a mode commonly referred to as off-axis sputtering (see "Methods" for details). We also rotated substrates with a constant speed. This gives rise to a radial variation of the IEC, while no obvious radial variations in interface roughness, crystalline structures and compositions of the deposited $Co_{40}Fe_{40}B_{20}$ have been observed in experimental measurements[25]. The in-plane asymmetry of the IEC is the origin of the interlayer DMI, as schematically shown in Fig. 1. This is in analogy to the situation of small spin clusters[8]. If we focus on one coupled pair of atoms in the two magnetic layers near the interfaces, the interlayer DMI that is mediated by the left segment of the magnetic thin film and that by the right segment cannot be compensated with each other, leading to a nonzero net interlayer DMI vector ($\mathbf{D}_{Int}$) acting on this pair of atoms. $\mathbf{D}_{Int}$ should be perpendicular to the axis of the in-plane asymmetry of the IEC, as suggested by the three-site Lévy–Fert model[31]. The

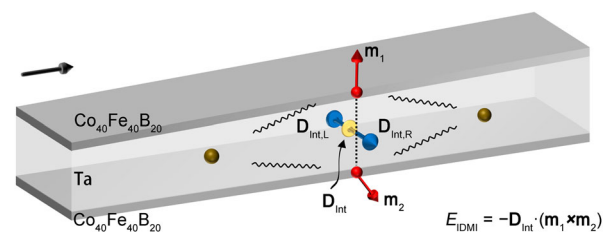$$E_{IDMI} = -\mathbf{D}_{Int} \cdot (\mathbf{m}_1 \times \mathbf{m}_2)$$

Fig. 1 Schematic of interactions between ferromagnetic layers that are separated by a nonmagnetic spacer. Wavy lines represent exchange interactions between localized spins (red balls and arrows) in ferromagnetic layers mediated by conduction electrons (dark gold balls) in the spacer. If we focus on one pair of atoms in ferromagnetic layers, because of the in-plane asymmetry of the interlayer exchange coupling (IEC) (black arrow along which the spacer-layer and ferromagnetic-layer thicknesses increase with a rate of 0.75%/mm and 0.77%/mm, respectively), the interlayer Dzyaloshinskii–Moriya interaction (DMI) that is mediated by the left part of magnetic thin films ($\mathbf{D}_{Int,L}$, blue arrow) and that is mediated by the right part of magnetic thin films ($\mathbf{D}_{Int,R}$, blue arrow) cannot be compensated with each other, leading to a nonzero net interlayer DMI vector ($\mathbf{D}_{Int}$, yellow arrow). The interlayer DMI governs a chiral magnetization across magnetic multilayers to lower the interlayer DMI energy $E_{IDMI} = -\mathbf{D}_{Int} \cdot (\mathbf{m}_1 \times \mathbf{m}_2)$, where $\mathbf{m}_1$ and $\mathbf{m}_2$ are magnetizations of the top and bottom ferromagnetic layers, respectively.

interlayer DMI favors a chiral magnetization across magnetic multilayers to lower the interlayer DMI energy $E_{\text{IDMI}} = -\mathbf{D}_{\text{Int}} \cdot (\mathbf{m}_1 \times \mathbf{m}_2)$ where $\mathbf{m}_1$ and $\mathbf{m}_2$ are magnetizations of the top and bottom ferromagnetic layers, respectively.

Demonstration of the existence of the interlayer DMI. To characterize the magnetic properties of the SAF, we applied an in-plane current along the long stripe of each Hall bar and measured the Hall resistance R_H through two 5-μm-wide leads. In the following, we will discuss the results obtained from Hall bars with the long axis aligned along the direction of the in-plane asymmetry. For our samples, the Hall resistance is dominated by an anomalous part proportional to the perpendicular magnetization M_z, while the much smaller part proportional to the perpendicular magnetic field H_z can be neglected in the interpretation[32]. Figure 2a shows the Hall resistance R_H results as a function of H_z for the SAF. There is a square loop around the zero magnetic field. Within this loop, the two ferromagnetic layers are antiferromagnetically coupled via the dominant RKKY interaction[25]. The magnetization has opposite normal components for the two layers. Besides, a finite in-plane component of magnetization should also be present because of the weak magnetic anisotropy of the thicker bottom layer. The almost antiparallel magnetization transforms into parallel magnetization on increasing or decreasing the perpendicular magnetic field. This process is

referred to as the spin-flop transition along which the Zeeman energy overcomes the IEC energy as discussed elsewhere[23–25]. In the following, we will focus on the switching between the two antiparallel magnetization states around zero magnetic field. It has been shown experimentally that, if the interlayer DMI is present, with the application of an in-plane magnetic field that is non-collinear with the interlayer DMI vector, the two almost antiparallel magnetization states are distinguished in their canting angles, hence, exhibiting different energy barriers for magnetization switching between the two states. This causes an asymmetric field-driven switching, and the asymmetry is angularly dependent on the direction of the in-plane magnetic field[9,10]. To demonstrate the presence of the interlayer DMI, we performed Hall resistance measurements on the SAF, while applying an in-plane magnetic field $\mathbf{H}_{\text{IP}}$.

As shown in Fig. 2c, field-induced magnetization switching becomes asymmetric under $H_{\text{IP}} = 100$ Oe along $\phi_H = 90°$ ($+y$ axis) vis-à-vis $\phi_H = 270°$($-y$ axis). Here, ϕ_H is the in-plane field angle relative to the x axis (see Fig. 2b). The perpendicular magnetic field bias, defined as $H_B = \frac{1}{2}(H_{c1} + H_{c2})$, where H_{c1} and H_{c2} are, respectively, negative and positive switching fields between two opposite spin states, is positive ($H_B = 3.5$ Oe) and negative ($H_B = -8.0$ Oe) for $\mathbf{H}_{\text{IP}} \| \phi_H = 90°$ and $\mathbf{H}_{\text{IP}} \| \phi_H = 270°$, respectively. We have measured the complete azimuthal angle ϕ_H dependence of H_B to reveal the asymmetric axis for magnetization
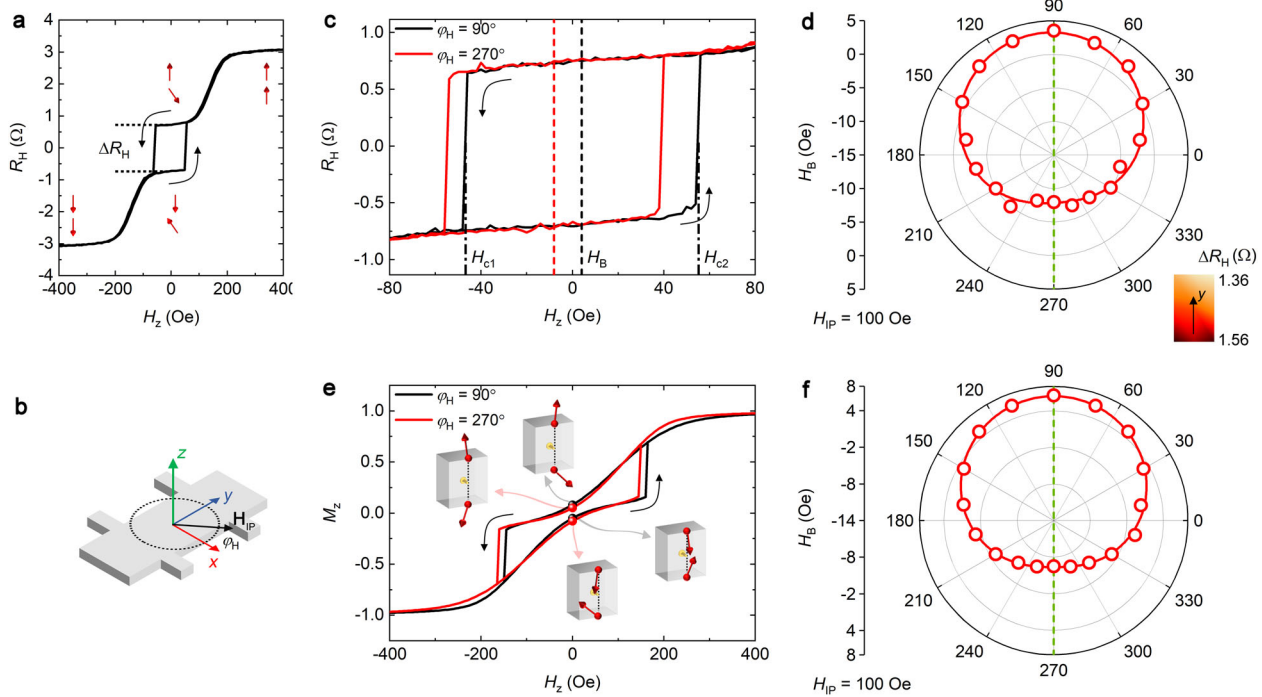

Fig. 2 Asymmetric field-driven switching of magnetization. a Hall resistance R_H versus perpendicular magnetic field H_z for the synthetic antiferromagnet (SAF). The anomalous Hall part of R_H that is proportional to the perpendicular magnetization M_z is dominant in the interpretation. Red arrows in the inset show the schematic of magnetic configurations at different stages during the Hall resistance measurement. The top and bottom red arrows represent magnetizations of the top and bottom ferromagnetic layers, respectively. **b** The schematic Hall bar structure with the definition of ϕ_H that is the relative angle between the in-plane field $\mathbf{H}_{\text{IP}}$ and the x axis. **c** Asymmetric hysteresis loops measured when applying an in-plane magnetic field $H_{\text{IP}} = 100$ Oe along $\phi_H = 90°$ (black) and $\phi_H = 270°$ (red). Dash-dotted lines indicate positions for negative (H_{c1}) and positive (H_{c2}) switching fields for $H_{\text{IP}} \| \phi_H = 90°$. Dashed lines indicate positions of field biases for $\mathbf{H}_{\text{IP}} \| \phi_H = 90°$ (black) and $\mathbf{H}_{\text{IP}} \| \phi_H = 270°$ (red). **d** ϕ_H dependence of the field bias H_B. Open dots are experimental data and the line is fitted by a cosine function $A_B \cos(\phi_H - \phi_{AS}) + B_B$ where A_B is the amplitude, ϕ_{AS} the angle for the asymmetric axis that is represented by the dashed line, B_B the offset of the field bias. The insert shows the spatial distributions of ΔR_H which reflects the in-plane asymmetry of interlayer exchange coupling (IEC) along the y axis. **e** Numerical calculations of asymmetric hysteresis loops for M_z when applying $H_{\text{IP}} = 100$ Oe along $\phi_H = 90°$ (black) and $\phi_H = 270°$ (red). The interlayer Dzyaloshinskii–Moriya interaction (DMI) vector $\mathbf{D}_{\text{Int}}$ along the $-x$ axis with the amplitude of $D_{\text{Int}} = -0.1 A_{\text{Int}}$ was adopted in calculations. The insert is the schematic of magnetic configurations for different spin states at zero perpendicular field and at the in-plane field of $\mathbf{H}_{\text{IP}} \| \phi_H = 90°$ and $\mathbf{H}_{\text{IP}} \| \phi_H = 270°$, respectively. **f** ϕ_H dependence of the field bias H_B derived from the numerical calculation. Open dots are numerical calculation results and the line is fitted by a cosine function $A_B \cos(\phi_H - \phi_{AS})$. Arrows represent switching directions.

switching. Figure 2d shows that the field bias is asymmetric along the y axis, which is consistent with the axis of the in-plane asymmetry of the IEC. The in-plane asymmetry can be confirmed through the spatial distributions of ΔR_H that is the Hall resistance difference of the two opposite spin states at zero field, as shown in the insert in Fig. 2d. ΔR_H decreases along the y direction that is the direction along which the Ta spacer thickness increases (see Supplementary Note 1 for more details).

We have also measured other Hall bars oriented along different directions to confirm that the asymmetric dependence of H_B on ϕ_H is related to the in-plane asymmetry, as shown in Supplementary Fig. 3 and discussed in Supplementary Note 2. The in-plane asymmetry of the IEC induces a finite interlayer DMI, which stabilizes the chiral magnetization across magnetic multilayers and gives rise to the asymmetric dependence of H_B on $\mathbf{H}_{IP}$. The tilt of easy axes of magnetic layers can also induce asymmetric field-driven switching; however, it would lead to the H_B sign change as varying the $\mathbf{H}_{IP}$ value, which is contrary to our experimental observations that the H_B sign only depends on the $\mathbf{H}_{IP}$ direction, as shown in Supplementary Fig. 4 and discussed in Supplementary Note 3 in detail.

The ϕ_H dependence of H_B in Fig. 2d implies that the interlayer DMI vector $\mathbf{D}_{Int}$ is along $-x$ axis for our Hall bar setup with the long axis along the y axis, which is also along the axis of the in-plane asymmetry. The magnetization prefers to be in the plane normal to the interlayer DMI vector to lower the interlayer DMI energy. The field-driven magnetization switching is the most asymmetric when $\mathbf{H}_{IP}$ is in the magnetization plane which can lead to the greatest difference in the canting between the two opposite magnetization states.

To confirm our analysis of the experimental data shown in Fig. 2c and d, we have computed the magnetization M_z as a function of H_z through minimization of the total free energy,

$$E_{tot} = -\mu_0(M_1 d_1 \mathbf{H}_{ext} \cdot \mathbf{m}_1 + M_2 d_2 \mathbf{H}_{ext} \cdot \mathbf{m}_2) - K_{u1} d_1 (\mathbf{m}_1 \cdot \mathbf{e}_z)^2$$
$$- K_{u2} d_2 (\mathbf{m}_2 \cdot \mathbf{e}_z)^2 - A_{Int}(\mathbf{m}_1 \cdot \mathbf{m}_2) - \mathbf{D}_{Int} \cdot (\mathbf{m}_1 \times \mathbf{m}_2). \quad (1)$$

In Eq. (1), μ_0 is the vacuum permeability, $\mathbf{H}_{ext} = \mathbf{H}_{IP} + H_z \mathbf{e}_z$ the external magnetic field and $\mathbf{e}_i$ ($i = x$, y, or z) the unit vector along the i axis. $\mathbf{m}_1$ and $\mathbf{m}_2$ are in the spherical coordinate with polar angles θ_1 and θ_2, azimuthal angles ϕ_1 and ϕ_2, respectively. The parameters we used are saturation magnetizations $M_1 = M_2 = 1.06 \times 10^6$ A m^{-1}, effective perpendicular magnetic anisotropies $K_{u1} = 0.94 \times 10^4$ Jm^{-3}, $K_{u2} = -0.80 \times 10^3$ Jm^{-3}, the RKKY coupling energy $A_{Int} = -1.07 \times 10^{-5}$ Jm^{-2} and the interlayer DMI with the vector pointing along $-x$ direction with the amplitude $D_{Int} = -0.1 A_{Int}$. Subscripts 1 and 2 refer to the top and bottom ferromagnetic layers, respectively. The M_z is then given by $M_z = \frac{M_1 d_1 \mathbf{m}_1 \cdot \mathbf{e}_z + M_2 d_2 \mathbf{m}_2 \cdot \mathbf{e}_z}{M_1 d_1 + M_2 d_2}$, where d_1 and d_2 are top and bottom ferromagnetic-layer thicknesses, respectively. In calculations of M_z as a function of H_z, we took $H_{IP} = 100$ Oe. The calculation results for M_z as shown in Fig. 2e well reproduce qualitatively the asymmetric feature of the Hall resistance results in Fig. 2c and also yield the result that the field bias is positive for $\mathbf{H}_{IP}\|\phi_H = 90°$, and negative for $\mathbf{H}_{IP}\|\phi_H = 270°$. Figure 2f shows the calculation result of ϕ_H dependence of H_B, which again well reproduces the experimental result in Fig. 2d that H_B shows an asymmetric $\mathbf{H}_{IP}$-dependence.

Asymmetric current-driven switching of magnetization. Having demonstrated the existence of the interlayer DMI and the chiral nature of magnetization in our SAF structure, we then studied the current-induced SOT switching of the chiral magnetization. In the previous section, we confirmed through the

field bias of the Hall resistance measurement that the interlayer DMI vector $\mathbf{D}_{Int}$ is along $-x$ axis, perpendicular to the direction of in-plane asymmetry along the y axis. To apply the spin torque, we passed an in-plane charge current $\mathbf{J}_e$ along the long stripe of the Hall bar to the multilayer stack. The Ta spacer converts the charge current to spin current. The spin current with opposite spin polarizations $\mathbf{m}_{p1} = \frac{\mathbf{e}_z \times \mathbf{J}_e}{J_e}$ and $\mathbf{m}_{p2} = -\mathbf{m}_{p1}$, respectively flows up and flows down along the z axis[5,28,33], exerting opposite SOTs on magnetizations in the two ferromagnetic layers. The SOTs on magnetization include the field-like torque $\boldsymbol{\tau}_{FL} = \mathbf{m} \times \mathbf{H}_{FL} = \zeta_{FL}\mathbf{m} \times \mathbf{m}_p$ and damping-like torque $\boldsymbol{\tau}_{DL} = \mathbf{m} \times \mathbf{H}_{DL} = \zeta_{DL}(\mathbf{m} \times (\mathbf{m} \times \mathbf{m}_p))$ where $\mathbf{H}_{FL} = \zeta_{FL}\mathbf{m}_p$ and $\mathbf{H}_{DL} = \zeta_{DL}(\mathbf{m} \times \mathbf{m}_p)$ are corresponding effective fields. ζ_{FL} and ζ_{DL} are the field-like torque coefficient and a damping-like torque coefficient, respectively. The SOTs can promote magnetizations in the two layers to rotate in opposite directions, and lead to the magnetization switching at moderate conditions.

We recorded changes in R_H while sweeping the current under different in-plane magnetic fields along the y axis (see "Methods" for details). The current has a pulse width of 1 ms. It has been shown experimentally that the emergence of edge domain walls would result in asymmetric SOT switching[34]. To avoid the effects of edge domain walls, we applied negative or positive perpendicular saturation fields to align magnetizations to the single-domain state before sweeping the current from 0 to 17 mA, or from 0 to −17 mA. The positive current refers to the current along the y axis and the negative to the $-y$ axis. There is no magnetization switching in the absence of an in-plane magnetic field within this range of applied current, as observed in many other systems[35,36]. As presented in Fig. 3a and b, deterministic magnetization switching by the current is achieved at $H_{IP} = \pm130$ Oe. The switching is clockwise for the negative H_{IP} ($\mathbf{H}_{IP}\|\phi_H = 270°$) and anticlockwise for the positive H_{IP} ($\mathbf{H}_{IP}\|\phi_H = 90°$), similar to that observed in Ta/CoFeB/MgO[28,29,33]. The absolute value of the negative switching current I_{c1} (−13.77 mA for $H_{IP} = -130$ Oe, −14.11 mA for $H_{IP} = 130$ Oe) is larger than the positive switching current I_{c2} (13.43 mA for $H_{IP} = -130$ Oe, 12.41 mA for $H_{IP} = 130$ Oe). This shows that the current-driven switching is asymmetric with a negative current bias $I_B = \frac{1}{2}(I_{c1} + I_{c2})$ (−0.17 mA for $H_{IP} = -130$ Oe, −0.85 mA for $H_{IP} = 130$ Oe).

To gain an understanding of the SOT switching, we have performed numerical calculations using the Landau–Lifshitz–Gilbert (LLG) equation,

$$\frac{d\mathbf{m}_1}{dt} = -\gamma\mathbf{m}_1 \times \mathbf{H}_{eff1} + \alpha_D \mathbf{m}_1 \times \frac{d\mathbf{m}_1}{dt} + \gamma\zeta_{DL}\mathbf{m}_1$$
$$\times (\mathbf{m}_1 \times \mathbf{m}_{p1}) + \gamma\zeta_{FL}\mathbf{m}_1 \times \mathbf{m}_{p1},$$
$$\frac{d\mathbf{m}_2}{dt} = -\gamma\mathbf{m}_2 \times \mathbf{H}_{eff2} + \alpha_D \mathbf{m}_2 \times \frac{d\mathbf{m}_2}{dt} + \gamma\zeta_{DL}\mathbf{m}_2$$
$$\times (\mathbf{m}_2 \times \mathbf{m}_{p2}) + \gamma\zeta_{FL}\mathbf{m}_2 \times \mathbf{m}_{p2}, \quad (2)$$

where $\mathbf{H}_{eff} = -\mathbf{e}_\theta \frac{\partial E_{tot}}{\mu_0 M d \partial \theta} - \mathbf{e}_\varphi \frac{\partial E_{tot}}{\mu_0 M d \sin\theta \partial\varphi}$. $\mathbf{e}_\theta$ is the unit vector of the polar angle θ and $\mathbf{e}_\phi$ is the unit vector of the azimuthal angle ϕ. γ is the gyromagnetic ratio. α_D is the Gilbert damping that was adopted to be 0.02. In calculations of the SOT switching, we adopted as before the same parameter $D_{Int} = -0.1 A_{Int}$ with $\mathbf{D}_{Int}$ vector along the $-x$ axis. The vertical magnetic field was set to zero and $H_{IP} = \pm130$ Oe. We adopted the same values of ζ_{FL} and $\zeta_{DL} = \zeta$ that are normalized by $K_{u1}/\mu_0 M_1$. Figure 3c and d show the calculation results of M_z with the same definition as before. The numerical calculations that incorporate the interlayer DMI reproduce both the switching direction that depends on the sign of H_{IP}, and the asymmetric feature of the switching that has a negative torque bias ζ_B.
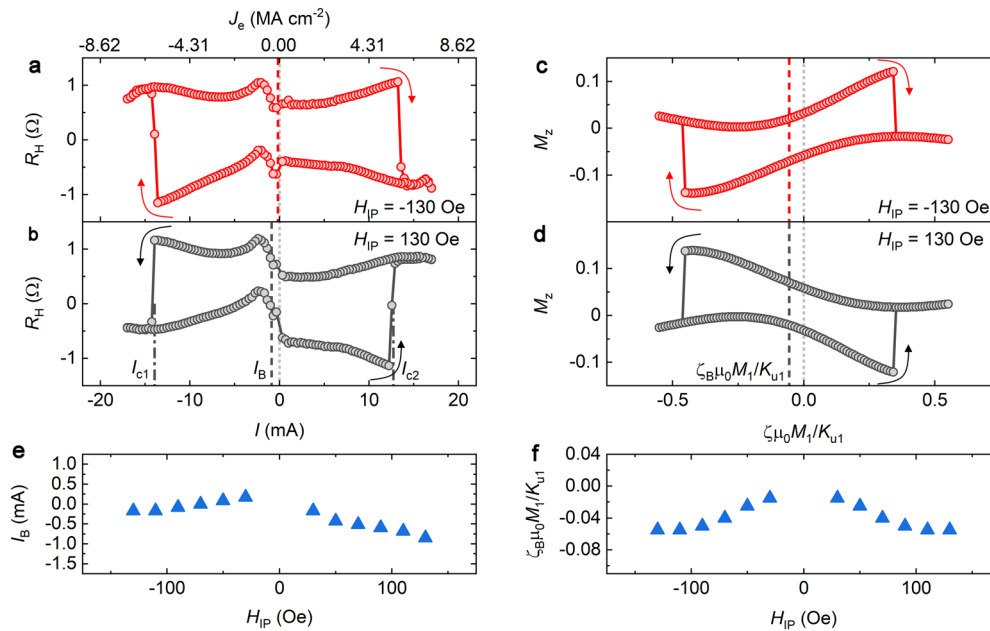
Fig. 3 Asymmetric current-driven switching of magnetization. a, b Current-driven magnetization switching with the application of a (**a**) negative and (**b**) positive H_{IP}. The anomalous Hall part of the Hall resistance R_H that is proportional to the perpendicular magnetization M_z is dominant in the interpretation. Positive values of current and field refer to corresponding vectors pointing along the y axis and negative to the $-y$ axis. Dash-dotted lines in (**b**) indicate positions of the negative (I_{c1}) and positive (I_{c2}) switching currents for the positive H_{IP}. Dashed lines indicate positions of the switching current biases I_B for a positive (black) and negative (red)H_{IP}. **c, d** Numerical calculations of the asymmetric SOT switching, with the application of a (**c**) negative and (**d**) positive H_{IP}. The interlayer Dzyaloshinskii–Moriya interaction (DMI) vector $\mathbf{D}_{Int}$ along the $-x$ axis with the amplitude of $D_{Int} = -0.1A_{Int}$ was adopted in calculations. **e** The current bias I_B as a function of H_{IP}. **f** Numerical calculations of the torque bias ζ_B as a function of H_{IP}. Arrows represent switching directions.

We have also measured the current bias as a function of H_{IP} as shown in Fig. 3e. The experimental results that I_B decreases with increasing $|H_{IP}|$ and the I_B value has the in-plane field reversal symmetry are again reproduced qualitatively by the numerical calculations as shown in Fig. 3f. The small asymmetric part in Fig. 3e is most probably attributed to the edge domain walls that may not be fully removed[34]. After extracting the asymmetric part of I_B with respect to H_{IP}, the results fit reasonably well with calculations that incorporate the interlayer DMI while the results cannot be reproduced even qualitatively by the tilted easy axes' model as shown in Supplementary Fig. 5. We have conducted similar experimental performance on a Hall bar with the long axis 90° away from the in-plane asymmetry, as well as on a single ferromagnetic-layer system. The results, as shown in Supplementary Fig. 7, are similar for the two systems, without a monotonous variation of I_B as a function $|H_{IP}|$, which are different from that shown in Fig. 3e and f, as discussed in Supplementary Note 5.

Joule heating would have an effect on current-driven switching. Comparing changes in longitudinal resistance as varying the temperature and varying the amplitude of current pulses, the temperature rise was estimated to be ~100 K around the switching current. However, we note that, if there is no Joule heating, the current bias effect would be even larger than that observed in Fig. 3a, b, and e, as discussed in Supplementary Note 6.

Discussion and conclusions

In recent works[9,10], authors reported experimental observations of field-biased hysteresis loops as a result of the interlayer DMI across magnetic multilayer stacks. In our work, we demonstrated the existence of the interlayer DMI in a different multilayer system with the in-plane asymmetry of the IEC, and then further studied the interlayer DMI's effects on current-driven magnetization switching. The interlayer DMI not only breaks the in-plane field reversal symmetry for perpendicular magnetic field-induced

magnetization switching but also induces different responses of two opposite spin states to SOTs, giving rise to asymmetric current-driven switching under an in-plane magnetic field. This can be utilized to design SOT devices with selective switching capability that can be tuned by the in-plane magnetic field.

We note that, in the field-driven switching (Fig. 2c), the high-R_H state switches into the low-R_H state at a lower field for $\mathbf{H}_{IP}\|\phi_H = 90°$ and at a higher field for $\mathbf{H}_{IP}\|\phi_H = 270°$, while in the current-driven switching (Fig. 3a, b), it occurs at a higher current for $\mathbf{H}_{IP}\|\phi_H = 90°$ and at a lower current for $\mathbf{H}_{IP}\|\phi_H = 270°$. The asymmetric field-driven switching can be understood by different energy barriers determined by the canting of magnetizations[9,10]. The magnetization of the high-R_H state is more canted compared to the magnetization of low-R_H state for $\mathbf{H}_{IP}\|\phi_H = 90°$ and is less canted for $\mathbf{H}_{IP}\|\phi_H = 270°$ (the inset in Fig. 2e). However, this cannot explain the asymmetric current-driven switching in Fig. 3. The sign of spin torques arising from the interlayer DMI depends on the magnetic configuration. In the switching process, the spin torque arising from the interlayer DMI switches its direction from antiparallel to parallel, or from parallel to antiparallel, to the direction of the damping-like torque, respectively, promoting or hindering the switching of magnetization, which is discussed in Supplementary Note 7 in detail.

One expects that through increasing the interlayer DMI's contributions to the total energy, that is, either increasing the interlayer DMI strength or decreasing the RKKY interaction strength and anisotropies of magnetic layers, the interlayer DMI's effects on the magnetization and its switching can increase (see Supplementary Fig. 12). This can be achieved by fabricating SAFs using materials with large antisymmetric/symmetric exchange interaction ratios[37], as well as by fabricating SAFs with magnetizations near the spin reorientation transition and near the transition from antiferromagnetic coupling to the ferromagnetic coupling between the magnetic layers. In our SAF structure, magnetizations are single domains. However, one would expect

that, if domain walls are present, the domain-wall motion would be asymmetric as a function of SOTs. The domain wall would move along one direction with a higher velocity when applying a current, while it moves along the opposite direction with a lower velocity when reversing the current direction. In previous studies[15], the asymmetric domain-wall motion was only reported as a function of the in-plane magnetic field. The current-controlled asymmetric domain-wall motion, if it is demonstrated, can provide a novel function to design racetrack memory and domain-wall-based spin logic devices. The interlayer DMI, together with the interfacial DMI, provides avenues to design and control 3D spin textures in magnetic heterostructures. The interplay of the interlayer DMI[11] with the RKKY exchange[38] also allows tuning of spin textures in different magnetic layers, possibly giving rise to novel chiral structures and physical properties. Our studies pave the way towards explorations on controlling the chiral magnetization in magnetic multilayers through SOTs.

Methods

Sample growth, fabrication, and characterization. The SAFs were grown on thermally oxidized silicon wafers using a high-vacuum magnetron sputtering system with a base vacuum pressure of 5.0×10^{-8} Torr. In depositions of magnetic thin films, the circular sputter source is parallel to the substrate, facing upwards and downwards, respectively. The vertical distance between the sputter source and substrate is 3.5 inches, and the center of the substrate is horizontally 1.25-inch away from the center of the sputter source. The self-rotation speed of the substrate is approximately 83 rpm. In magnetic thin films, the MgO layers were deposited using radio-frequency (RF) power under an argon pressure of 0.7 mTorr and other layers were deposited using DC power under an argon pressure of 1.4 mTorr. We used 3 Watt of DC power for the deposition of Ta layers and 15 Watt of DC power for the deposition of ferromagnetic $Co_{40}Fe_{40}B_{20}$ layers. The deposition rates for different layers were calibrated by X-ray reflectivity measurements using the Bruker D8 Discover X-ray diffractometer[25]. We patterned samples into Hall bars (20×140 μm) using photolithography and physical ion milling. The samples were then annealed at different temperatures in a high-vacuum chamber with the vacuum pressure of $\sim 1.0 \times 10^{-6}$ Torr under a magnetic field of ~ 0.4 T normal to the sample plane.

We used a wire-bonder machine (HB10, TPT) to bond the sample and pads on a PCB board for Hall resistance measurements. The Hall resistance measurements were performed at room temperature under two pairs of electromagnets that have been well-calibrated. We used a Keithley 6221 current source to apply a DC current or current pulses. The DC current with the amplitude of 0.1 mA was applied for measuring the Hall resistance as a function of the field. Current pulses with a pulse width of 1 ms were applied for measuring the current-driven magnetization switching. In measurements, we connected the Hall voltage leads of the Hall bar to two voltmeters simultaneously. One is Keithley 199 for measuring field-driven switching and the other one is Keithley 2182A for measuring current-driven switching. During recording the Hall voltage using Keithley 2182A, the connection to the other voltmeter gives rise to the features around zero current in Fig. 3a and b. However, we note that this does not affect the current for magnetization switching, which has been confirmed through multiple tests on different samples. In Hall resistance measurement, the current flows in all Ta layers. Although all Ta layers can generate a spin current, only the middle Ta spacer layer contributes to the current-driven switching. This is because of the limited diffusion length of spin current and insulating properties of MgO layers. Similarly, we only took into consideration the spin current generated from the middle Ta spacer in our numerical calculations.

The in-plane magnetic field $\mathbf{H}_{IP}$ was confirmed in the sample plane through the Hall resistance measurements, as the switching of magnetization would be incomplete even when the field $\mathbf{H}_{IP}$ tilts vary slightly from the sample plane to the normal direction (see Supplementary Note 4 and Supplementary Fig. 6).

Data availability
The authors declare that the data supporting the findings of this study are available within the article and are available from the corresponding author upon reasonable request.

Code availability
The authors declare that all codes used for the analysis presented in this study are available from the corresponding author upon reasonable request.

References

1. Hellman, F. et al. Interface-induced phenomena in magnetism. *Rev. Mod. Phys.* **89**, 025006 (2017).
2. Wiesendanger, R. Nanoscale magnetic skyrmions in metallic films and multilayers: a new twist for spintronics. *Nat. Rev. Mater.* **1**, 16044 (2016).
3. Meier, T., Kronseder, M. & Back, C. Domain-width model for perpendicularly magnetized systems with Dzyaloshinskii-Moriya interaction. *Phys. Rev. B* **96**, 144408 (2017).
4. Woo, S. et al. Observation of room-temperature magnetic skyrmions and their current-driven dynamics in ultrathin metallic ferromagnets. *Nat. Mater.* **15**, 501 (2016).
5. Wang, K. et al. Spin torque effect on topological defects and transitions of magnetic domain phases in Ta/CoFeB/MgO. *Phys. Rev. B* **99**, 184410 (2019).
6. Legrand, W. et al. Room-temperature stabilization of antiferromagnetic skyrmions in synthetic antiferromagnets. *Nat. Mater.* **19**, 34–42 (2020).
7. Lee, A. J. et al. Probing the source of the interfacial Dzyaloshinskii-Moriya interaction responsible for the topological Hall effect in Metal/Tm 3Fe5O12 systems. *Phys. Rev. Lett.* **124**, 107201 (2020).
8. Vedmedenko, E. Y., Riego, P., Arregi, J. A. & Berger, A. Interlayer Dzyaloshinskii-Moriya interactions. *Phys. Rev. Lett.* **122**, 257202 (2019).
9. Fernández-Pacheco, A. et al. Symmetry-breaking interlayer Dzyaloshinskii–Moriya interactions in synthetic antiferromagnets. *Nat. Mater.* **18**, 679 (2019).
10. Han, D.-S. et al. Long-range chiral exchange interaction in synthetic antiferromagnets. *Nat. Mater.* **18**, 703 (2019).
11. Pollard, S. D. et al. Bloch chirality induced by an interlayer Dzyaloshinskii-Moriya interaction in ferromagnetic multilayers. *Phys. Rev. Lett.* **125**, 227203 (2020).
12. Jiang, W. et al. Blowing magnetic skyrmion bubbles. *Science* **349**, 283–286 (2015).
13. Yu, G. et al. Room-temperature creation and spin–orbit torque manipulation of skyrmions in thin films with engineered asymmetry. *Nano Lett.* **16**, 1981–1988 (2016).
14. Wang, K., Qian, L., Ying, S.-C., Xiao, G. & Wu, X. Controlled modification of skyrmion information in a three-terminal racetrack memory. *Nanoscale* **11**, 6952–6961 (2019).
15. Ryu, K.-S., Thomas, L., Yang, S.-H. & Parkin, S. Chiral spin torque at magnetic domain walls. *Nat. Nanotech.* **8**, 527 (2013).
16. Siddiqui, S. A., Han, J., Finley, J. T., Ross, C. A. & Liu, L. Current-induced domain wall motion in a compensated ferrimagnet. *Phys. Rev. Lett.* **121**, 057701 (2018).
17. Ryu, K.-S., Yang, S.-H., Thomas, L. & Parkin, S. S. Chiral spin torque arising from proximity-induced magnetization. *Nat. Commun.* **5**, 1–8 (2014).
18. Ando, F. et al. Observation of superconducting diode effect. *Nature* **584**, 373–376 (2020).
19. Grünberg, P., Schreiber, R., Pang, Y., Brodsky, M. & Sowers, H. Layered magnetic structures: evidence for antiferromagnetic coupling of Fe layers across Cr interlayers. *Phys. Rev. Lett.* **57**, 2442 (1986).
20. Parkin, S. S. Systematic variation of the strength and oscillation period of indirect magnetic exchange coupling through the 3d, 4d, and 5d transition metals. *Phys. Rev. Lett.* **67**, 3598 (1991).
21. Duine, R., Lee, K.-J., Parkin, S. S. & Stiles, M. D. Synthetic antiferromagnetic spintronics. *Nat. Phys.* **14**, 217 (2018).
22. Bruno, P. Theory of interlayer magnetic coupling. *Phys. Rev. B* **52**, 411 (1995).
23. Cheng, C.-W., Shiue, C., Cheng, T.-I. & Chern, G. Observation of parallel-antiparallel magnetic coupling in ultrathin CoFeB-MgO based structures with perpendicular magnetic anisotropy. *J. Appl Phys.* **112**, 033917 (2012).
24. Dieny, B., Gavigan, J. & Rebouillat, J. Magnetisation processes, hysteresis and finite-size effects in model multilayer systems of cubic or uniaxial anisotropy with antiferromagnetic coupling between adjacent ferromagnetic layers. *J. Phys. Condens Matter* **2**, 159 (1990).
25. Wang, K., Qian, L., Ying, S.-C. & Xiao, G. Manipulation of the interlayer exchange coupling in perpendicular magnetized thin films via tunable magnetic-layer and spacer thicknesses. *Phys. Rev. B* **102**, 144430 (2020).
26. Yang, H. et al. First-principles investigation of the very large perpendicular magnetic anisotropy at Fe| MgO and Co| MgO interfaces. *Phys. Rev. B* **84**, 054401 (2011).
27. Dieny, B. & Chshiev, M. Perpendicular magnetic anisotropy at transition metal/oxide interfaces and applications. *Rev. Mod. Phys.* **89**, 025008 (2017).
28. Hao, Q. & Xiao, G. Giant spin Hall effect and magnetotransport in a Ta/ CoFeB/MgO layered structure: a temperature dependence study. *Phys. Rev. B* **91**, 224413 (2015).
29. Qian, L., Wang, K., Zheng, Y. & Xiao, G. Spin Hall effect in the α and β phases of T a x W 1− x alloys. *Phys. Rev. B* **102**, 094438 (2020).
30. Wang, K., Zhang, Y. & Xiao, G. Anomalous Hall sensors with high sensitivity and stability based on interlayer exchange-coupled magnetic thin films. *Phys. Rev. Appl* **13**, 064009 (2020).

31. Levy, P. M. & Fert, A. Anisotropy induced by nonmagnetic impurities in Cu Mn spin-glass alloys. *Phys. Rev. B* **23**, 4667 (1981).

32. Nagaosa, N., Sinova, J., Onoda, S., MacDonald, A. H. & Ong, N. P. Anomalous Hall effect. *Rev. Mod. Phys.* **82**, 1539 (2010).

33. Liu, L. et al. Spin-torque switching with the giant spin Hall effect of tantalum. *Science* **336**, 555–558 (2012).

34. Zhao, X. et al. Asymmetric current-driven switching of synthetic antiferromagnets with Pt insert layers. *Nanoscale* **10**, 7612–7618 (2018).

35. Liu, L., Lee, O., Gudmundsen, T., Ralph, D. & Buhrman, R. Current-induced switching of perpendicularly magnetized magnetic layers using spin torque from the spin Hall effect. *Phys. Rev. Lett.* **109**, 096602 (2012).

36. An, H. et al. Current-induced magnetization switching using an electrically insulating spin-torque generator. *Sci. Adv.* **4**, eaar2250 (2018).

37. Romming, N. et al. Competition of Dzyaloshinskii-Moriya and higher-order exchange interactions in Rh/Fe atomic bilayers on Ir (111). *Phys. Rev. Lett.* **120**, 207201 (2018).

38. Lucassen, J. et al. Tuning magnetic chirality by dipolar interactions. *Phys. Rev. Lett.* **123**, 157201 (2019).

Acknowledgements

Author contributions

K.W. and G.X. conceived the research. G.X. supervised the experiments, K.W. and L.Q. performed the sample growth, fabrication, and characterizations. S.Y. supervised numerical calculations. K.W. performed numerical calculations. K.W. and L.Q. wrote the paper. All authors discussed the results and commented on the paper.

Competing interests

The authors declare no competing interests.

Additional information

Supplementary information is available for this paper at https://doi.org/10.1038/s42005-020-00513-z.

Correspondence and requests for materials should be addressed to K.W. or G.X.

Reprints and permission information is available at http://www.nature.com/reprints

Publisher's note Springer Nature remains neutral with regard to jurisdictional claims in published maps and institutional affiliations.